Paper No.
2380

NACE INTERNATIONAL CORROSION 2013 CONFERENCE & EXPO

Corrosion Behavior of Deep Water Oil Production Tubing Material under Supercritical CO_2 Environment: Part I. Effect of Pressure and Temperature

Yoon-Seok Choi
Institute for Corrosion and Multiphase Technology, Department of Chemical and Biomolecular Engineering, Ohio University
342 West State Street
Athens, OH 45701, USA

Fernando Farelas
Institute for Corrosion and Multiphase Technology, Department of Chemical and Biomolecular Engineering, Ohio University
342 West State Street
Athens, OH 45701, USA

Srdjan Nešić
Institute for Corrosion and Multiphase Technology, Department of Chemical and Biomolecular Engineering, Ohio University
342 West State Street
Athens, OH 45701, USA

Alvaro Augusto O. Magalhães
Petrobras
Av. Horacio Macedo, 950 – Cidade Universitaria, Ilha do Fundao, Rio de Janeiro, RJ 21941-915, Brazil

Cynthia de Azevedo Andrade
Petrobras
Av. Horacio Macedo, 950 – Cidade Universitaria, Ilha do Fundao, Rio de Janeiro, RJ 21941-915, Brazil

ABSTRACT

The objective of the present study is to evaluate the corrosion properties of carbon steel in supercritical CO_2/brine mixtures related to the deep water oil production development. Corrosion tests were performed in 25 wt.% NaCl solution under different CO_2 partial pressures (4, 8, 12 MPa) and temperatures (65, 90°C). Corrosion behavior of carbon steel was evaluated by using electrochemical methods (linear polarization resistance [LPR] and electrochemical impedance spectroscopy [EIS]), weight loss measurements and surface analytical techniques (scanning electron microscopy [SEM], energy dispersive X-ray spectroscopy [EDS], X-ray diffraction [XRD] and infinite focus microscopy [IFM]). The corrosion rates measured at 65°C showed a high corrosion rate (~ 10 mm/y) and slight difference with pressure. Under these conditions, the sample surface was locally covered by iron carbide (Fe_3C) which is porous and non-protective. However, the corrosion rates measured at 90°C increased with time at the initial period of the test and decreased to very low value (~ 0.05 mm/y) due to the formation of protective $FeCO_3$ layer regardless the CO_2 partial pressure.

Key words: supercritical CO_2, carbon steel, CO_2 corrosion, $FeCO_3$

INTRODUCTION

Demand for energy in the world is fueling non-conventional oil discoveries such as deep water production; this brings many challenges that have necessitated engineering changes, design adaptations and selection of alternative materials and systems.[1-3] A major issue in deep water production is corrosion and materials technology because of the extreme conditions (high pressure, high temperature, high CO_2 and high chloride).[4] Even though corrosion resistance alloy (CRA) has been available as a materials selection option for these severe environments, carbon and low alloy steels are still widely used as tubing materials because of their strength, availability and cost.[5-7]

The main difference between conventional oil production and deep water production is the reservoir pressure which exceeds 30 MPa often with significant amounts of CO_2.[1] Consequently, the CO_2 might be in its supercritical state if the temperature and the pressure are over 31.1°C and 7.38 MPa, respectively. Based on the literature, it is known that the corrosion rate of carbon steel under supercritical CO_2 without protective $FeCO_3$ is very high (≥ 20 mm/y).[8-12] At certain conditions, the corrosion rate can decrease to low values (< 1 mm/y) in long-term exposure due to the formation of a protective film of $FeCO_3$.[10-13] Although studies related to general aqueous CO_2 corrosion at high CO_2 pressures have been carried out and reported recently, there are no comprehensive studies available for crude oil/CO_2/brine environments at supercritical CO_2 condition.

The overall objective of the study was to evaluate corrosion behavior of carbon steel in crude oil/supercritical CO_2/brine mixtures related to the deep water oil production development. In the present study (part 1), the corrosion properties of carbon steel were evaluated under different CO_2 partial pressures (4, 8 and 12 MPa) and temperatures (65 and 90°C) in 25 wt.% NaCl solution. The part 2 study[14] aimed to evaluate the corrosion behavior of carbon steel exposed to crude oil/supercritical CO_2/brine mixtures at different water cuts (0, 30, 50, 70, and 100%) in a flowing 25 wt.% NaCl solution.

EXPERIMENTAL PROCEDURE

The test specimens were machined from carbon steel (API[(1)]5CT L80) with two different types: a rectangular type with a size of 1.27 cm × 1.27 cm × 0.254 cm for weight loss measurement and surface analysis, and a cylinder type with 4.94 cm^2 exposed area for electrochemical measurements. The composition of steel is given in Table 1. Prior to exposure, the specimens were ground with 600-grit silicon carbide (SiC) paper, cleaned with isopropyl alcohol in an ultrasonic bath, and dried.

Table 1
Element Analysis by Atomic Emission Spectroscopy for the Carbon Steel used in the Tests (wt.%)

C	Cr	Mn	P	S	Si	Fe
0.30	0.85	0.91	0.015	0.008	0.29	Balance

The corrosion experiments were carried out in a 4-liter static stainless steel autoclave which contained a working electrode, a high pressure/high temperature Ag/AgCl reference electrode and a platinum coated niobium counter electrode. Schematic of the autoclave with experimental set up is shown in Figure 1. All tests were conducted in 25 wt.% NaCl aqueous solution.

Table 2 shows the test conditions. During experiment, corrosion rates were monitored with LPR and EIS measurements made at regular time intervals. LPR measurements were performed in a range of ±5 mV with respect to the open circuit potential (OCP), and a scan rate of 0.125 mV/s. EIS measurements were conducted in the frequency range from 10 kHz to 10 mHz, with an AC signal

(1) American Petroleum Institute (API), 1220 L St. NW, Washington, DC 20005.

amplitude of 5 mV (rms) at the OCP. The polarization resistance (R_p) obtained from LPR and EIS techniques, was used to calculate the corrosion current density (i_{corr}) by using Eq. (1):

$$i_{corr} = \frac{B}{R_p} = \frac{\beta_a \times \beta_c}{2.3 \times R_p \times (\beta_a + \beta_c)} \quad (1)$$

where β_a is the anodic Tafel constant (40 mV/dec), β_c is the cathodic Tafel constant (120 mV/dec). Then, the i_{corr} was converted into corrosion rate using Eq. (2):

$$\text{Corrosion rate}(mm/year) = \frac{0.00327 \times i_{corr}(\mu A/cm^2) \times EW}{\text{density}(g/cm^3)} \quad (2)$$

where EW is the equivalent weight in grams and 0.00327 is a constant factor used for dimension and time conversion.

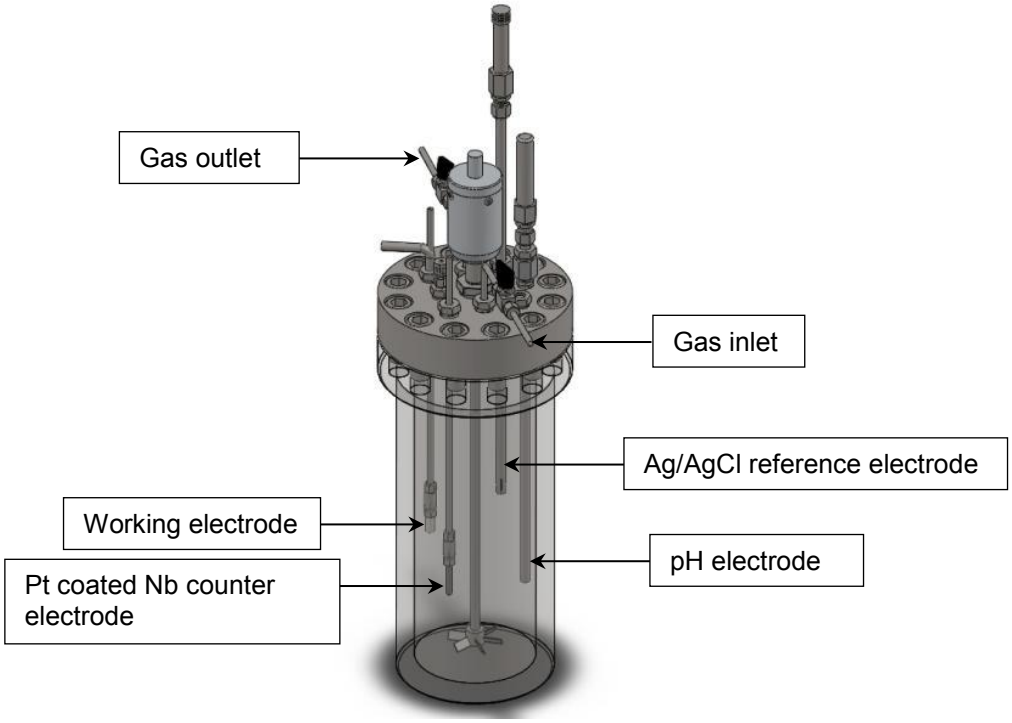

Figure 1: Schematic of autoclave system equipped for electrochemical measurements (stagnant condition without any agitation).

Table 2
Test Matrix for Corrosion Testing

	CO_2 pressure (MPa)		
Temperature (°C)	4	8	12
65	Gas phase	Supercritical Phase	Supercritical Phase
90	Gas phase	Supercritical Phase	Supercritical Phase

After the experiment, the specimen was taken to additional ex-situ analyses. The morphology and compositions of corrosion products were analyzed with SEM, EDS, XRD and IFM.

RESULTS

Experiments at 65°C

Figure 2 shows the variations of corrosion rate and OCP with time for carbon steel with different CO_2 partial pressures at 65°C. As shown in Figure 2 (a), the initial corrosion rate was about 5.5 mm/y for all three conditions; it increased with time for approximately one day and then stayed constant after that. At the end of the test the corrosion rates showed slight difference with pressure, i.e., it showed higher value at higher pressure. This behavior can be attributed to the concentration of carbonic acid (H_2CO_3) in the brine. As the partial pressure of CO_2 increases, the concentration of H_2CO_3 also increases, accelerating the cathodic reactions and therefore increasing the corrosion rate.[9,15] This can also be supported by the potential changes with time shown in Figure 2 (b). Slightly more noble potential was measured for higher CO_2 partial pressure conditions indicating higher cathodic reaction rate.

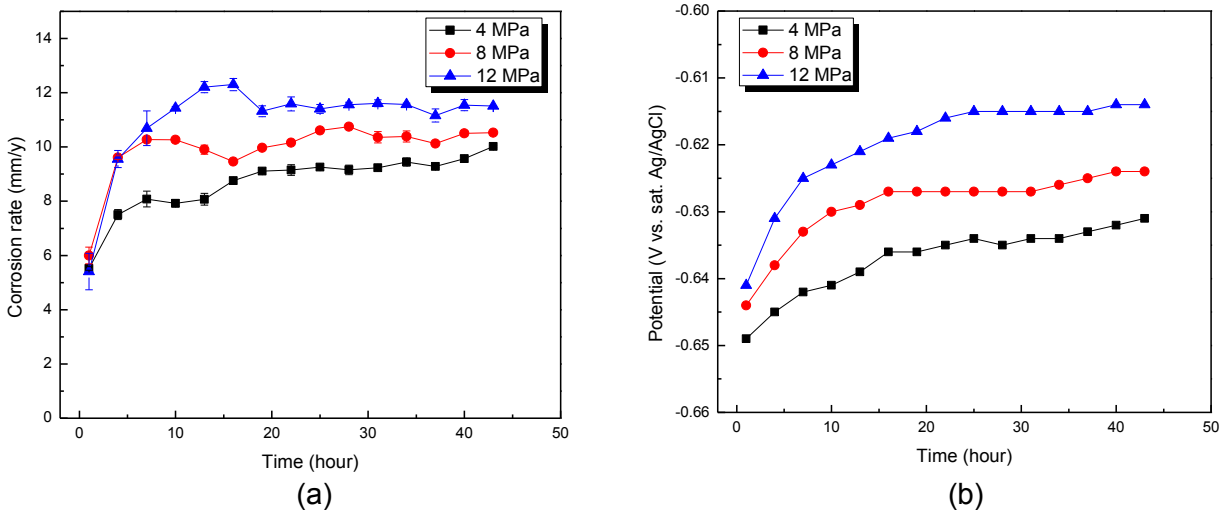

Figure 2: Variations of (a) corrosion rate and (b) corrosion potential with time for carbon steel with different CO_2 partial pressures at 65°C.

Figure 3 compares the average corrosion rate obtained from electrochemical and weight loss measurements under different CO_2 partial pressures. Under these experimental conditions, the corrosion rate measured by both techniques increased with pressure. The difference between them could be attributed to the approximate B value (13 mV) used for calculating the corrosion rate from the electrochemical measurements.

Figure 4 shows the SEM images of the sample surfaces after 48 hours of the exposure in the 25 wt.% NaCl solution at 65°C with different CO_2 partial pressures (4, 8 and 12 MPa). It can be seen that the morphologies were almost identical for different pressures and the surface was locally covered by the corrosion products.

Figure 5 shows the XRD pattern of the corrosion product layer formed at 12 MPa, 65°C. The layer formed in this condition showed dominant Fe_3C diffraction patterns with some $FeCO_3$. This indicated that the corrosion products shown in Figure 4 can be identified as Fe_3C. The Fe_3C initially present in the carbon steel is exposed after the preferential dissolution of ferrite (α-Fe) and accumulates on the steel surface; therefore it is non-protective, porous and easily spalls off from the steel substrate.[16]

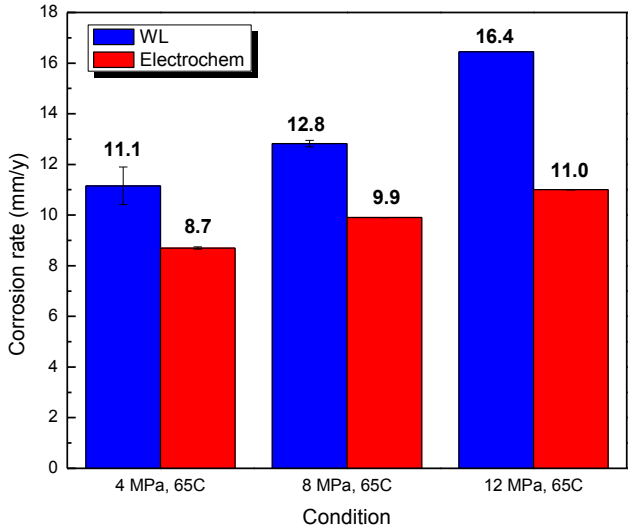

Figure 3: Comparison of corrosion rates obtained from weight loss and electrochemical measurements (time-averaged) with different CO_2 partial pressures at 65°C for 48 hours.

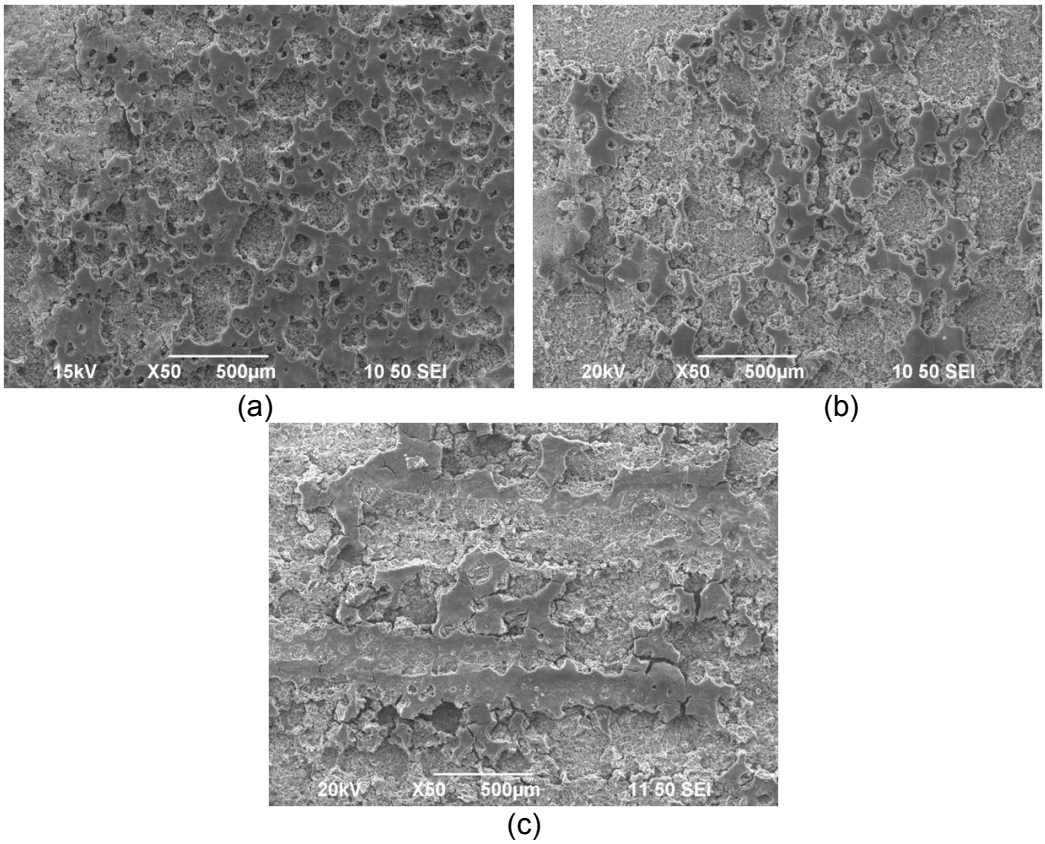

Figure 4: SEM images of the corroded surface of the samples exposed to 25 wt.% NaCl solution at 65°C: (a) 4 MPa, (b) 8 MPa and (c) 12 MPa.

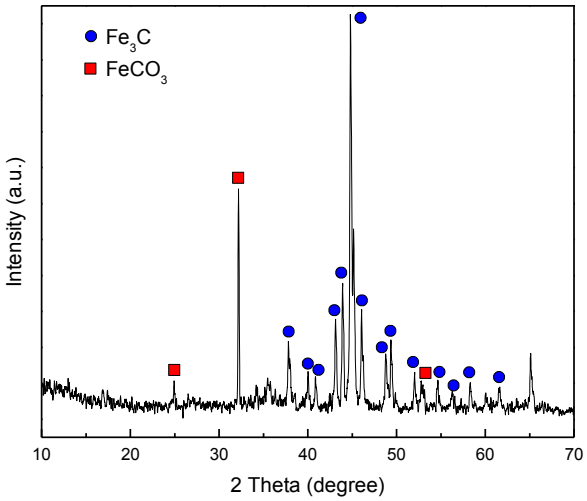

Figure 5: Result of XRD analysis for the sample exposed to 12 MPa, 65°C for 48 hours.

Figure 6 shows the surface morphologies of samples after cleaning with Clarke solution. It can be seen that severe uniform corrosion attack was observed on the surface for samples at 4 MPa and 8 MPa, i.e., there was no localized corrosion. This implies that even though the Fe_3C layer locally formed on the steel surface, it did not initiate localized corrosion. However, in the case of 12 MPa, pits were observed on the cleaned surface which may suggest localized corrosion under this condition. In order to measure a pit depth and calculate localized corrosion rate, infinite focus microscope (IFM) analysis was performed for all samples.

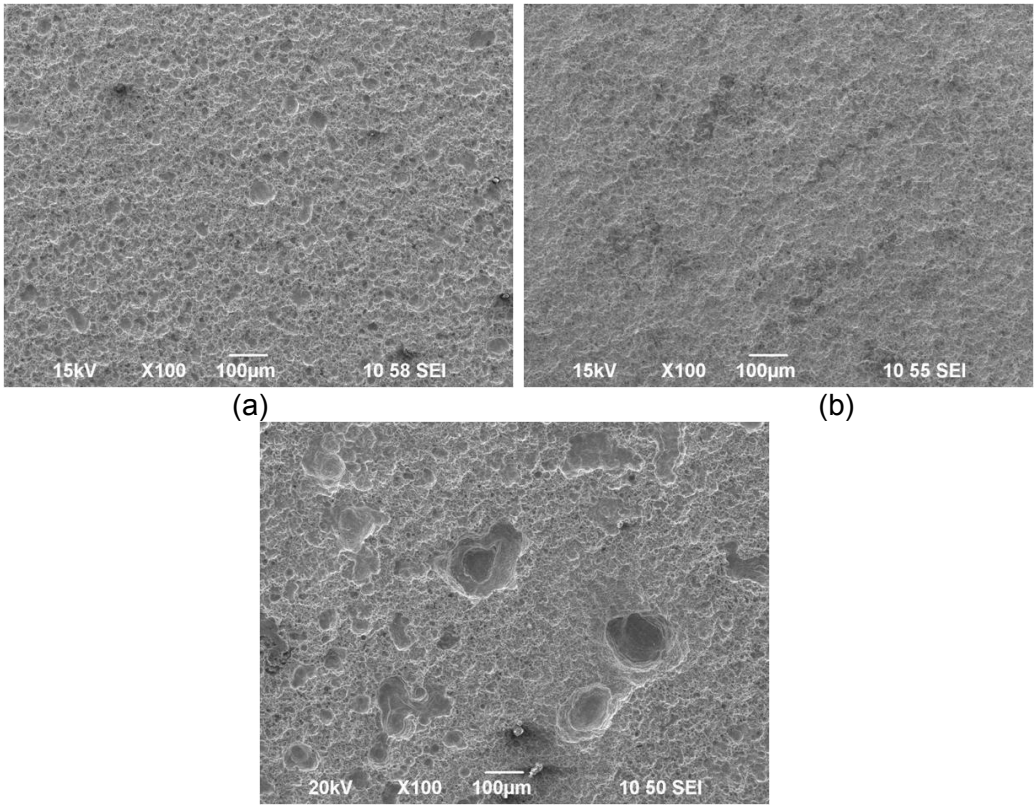

Figure 6: SEM images of the corroded surface of samples after cleaning: (a) 4 MPa, 65°C, (b) 8 MPa, 65°C and (c) 12 MPa, 65°C.

Figure 7 shows result of IFM analysis for the sample exposed to 12 MPa CO_2 partial pressure at 65°C and Table 3 compares the corrosion rate obtained from weight loss measurements and IFM analysis. In the cases of 4 MPa and 8 MPa, the pit penetration rate calculated from the maximum pit depth showed lower value than the uniform corrosion rate which confirms this corrosion type as uniform corrosion. At 12 MPa, the maximum pit depth was around 119 µm that corresponds to a pit penetration rate of 21.7 mm/y. This rate is similar to the uniform corrosion rate obtained from the weight loss measurement (16.4 mm/y) and this type of attack can be classified as severe uniform corrosion.

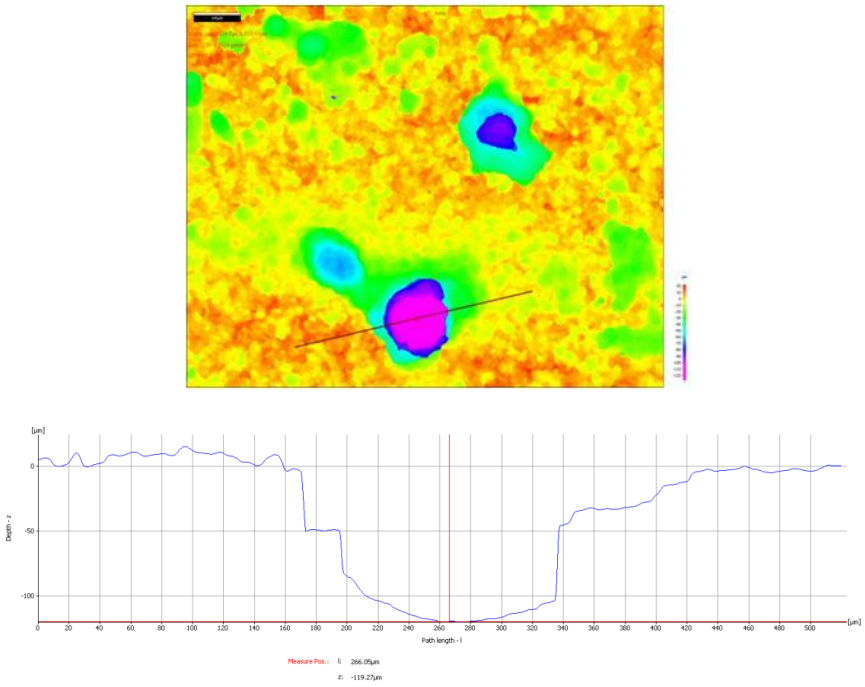

Figure 7: IFM surface analysis on cleaned surface of the sample exposed to 12 MPa, 65°C for 48 hours.

Table 3
Comparison of Corrosion Rates obtained from Weight Loss Measurements and IFM Analysis at 65°C for 48 hours

	Corrosion rate from weight loss (mm/y)	Maximum pit depth from IFM (µm)	Pit penetration rate (mm/y)
4 MPa	11.1	37.4	6.8
8 MPa	12.9	10.5	1.9
12 MPa	16.4	119.3	21.7

Experiments at 90°C

Figure 8 shows the variations of corrosion rate and OCP with time for carbon steel at different CO_2 partial pressures exposed for 43 hours at 90°C. At the beginning of the test, the corrosion rates increased for all three conditions. Higher corrosion rate was obtained for higher CO_2 partial pressure. Comparing the corrosion rates measured at 65°C and 90°C, the latter were much higher (almost double) during the first 7 hours of exposure. Subsequently, a rapid decrease in the corrosion rates can be seen for all three conditions, reaching a low corrosion rate (≤ 1 mm/y) at the end of 43 hours of exposure.

The increase in corrosion rate at the initial periods of the test could be ascribed to the formation of Fe_3C layer on the steel surface. It has been proved that Fe_3C is an electronic conductor so that its presence

on the steel surface increases the corrosion rate by a galvanic effect between the steel substrate and Fe_3C layer.[17] Furthermore, the increase in corrosion rate with pressure is due to an increase in the concentration of H_2CO_3 in the solution as the partial pressure of CO_2 increases.

The decrease in corrosion rates after 7 hours can be attributed to the formation of protective $FeCO_3$ layer. A more protective layer formed faster on the steel surface at higher CO_2 partial pressures. This is supported by a largest shift in the corrosion potential towards more noble values at 12 MPa (Figure 8 (b)).

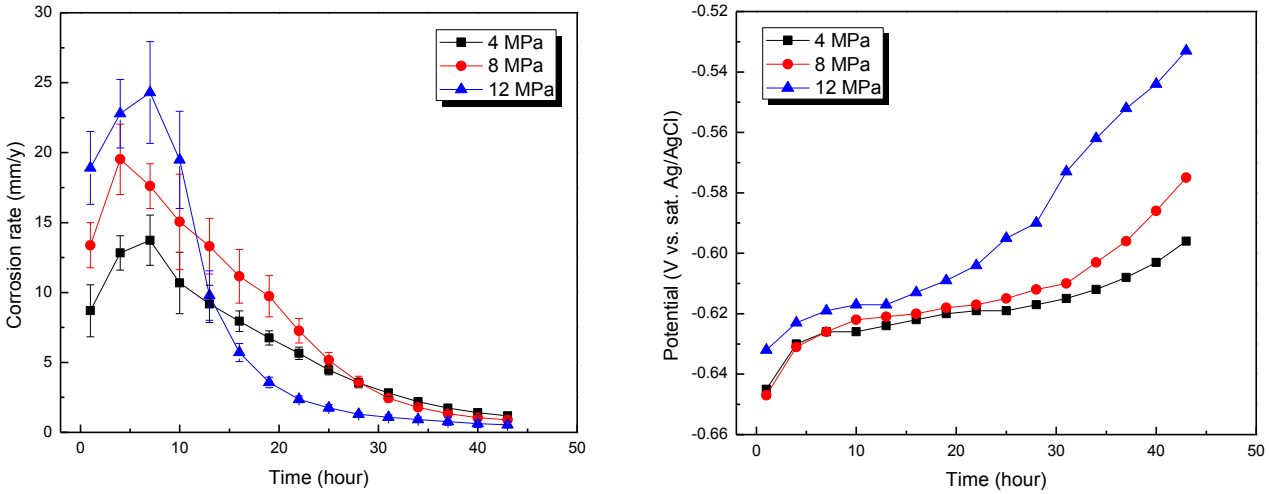

(a) (b)

Figure 8: Variations of (a) corrosion rate and (b) corrosion potential with time for carbon steel with different CO_2 partial pressures at 90°C.

Since the corrosion rates kept decreasing at 43 hours of exposure shown in Figure 8 (a), experiments at 8 and 12 MPa were continued until a stable corrosion rate was measured. Figure 9 shows the variations of corrosion rate and OCP for carbon steel with different CO_2 partial pressures at 90°C over an extended time. At 8 MPa the corrosion rate decreased up to 0.05 mm/y after 112 h of exposure, while at 12 MPa it decreased to 0.1 mm/y after 70 h of exposure. Due to the formation of the protective $FeCO_3$ layer, the corrosion potential shifted to more noble values and in both conditions a change of approximately 150 mV was observed.

Figure 10 compares the corrosion rates measured from weight loss measurements, and from LPR measurements (average). The corrosion rates from both techniques showed high values compare with the final corrosion rates because of the high corrosion rates at the initial periods of the tests.

SEM surface images of the samples are shown in Figure 11. It is interesting to note that for all three conditions, the surface does not appear to be fully covered by $FeCO_3$ even though very low corrosion rates were measured at 8 MPa and 12 MPa. However, the true coverage by the protective $FeCO_3$ layer can be properly judged only from cross sectional images, shown below.

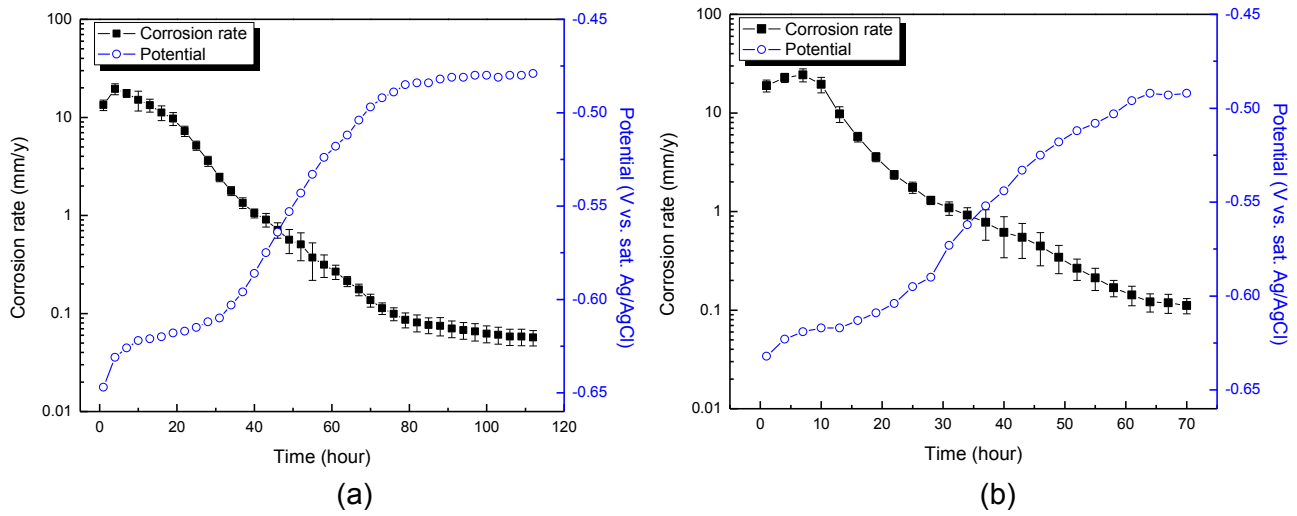

Figure 9: Variations of corrosion rate and corrosion potential with time for carbon steel with different CO_2 partial pressures at 90°C: (a) 8 MPa and (b) 12 MPa.

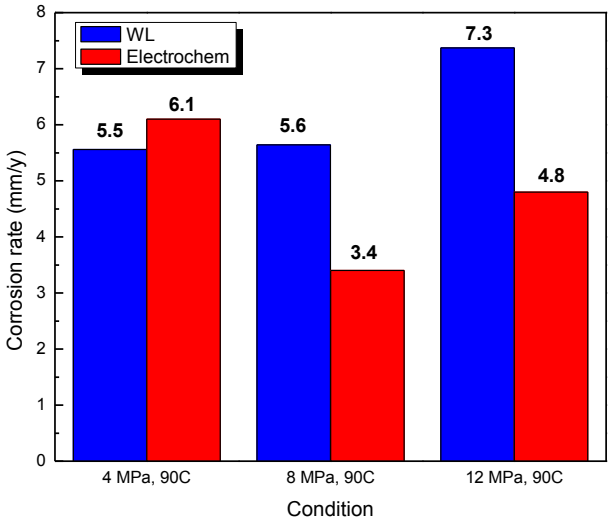

Figure 10: Comparison of corrosion rates obtained from weight loss and electrochemical measurements (average) with different CO_2 partial pressures at 90°C for 48 hours (4 MPa), 114 hours (8 MPa) and 72 hours (12 MPa).

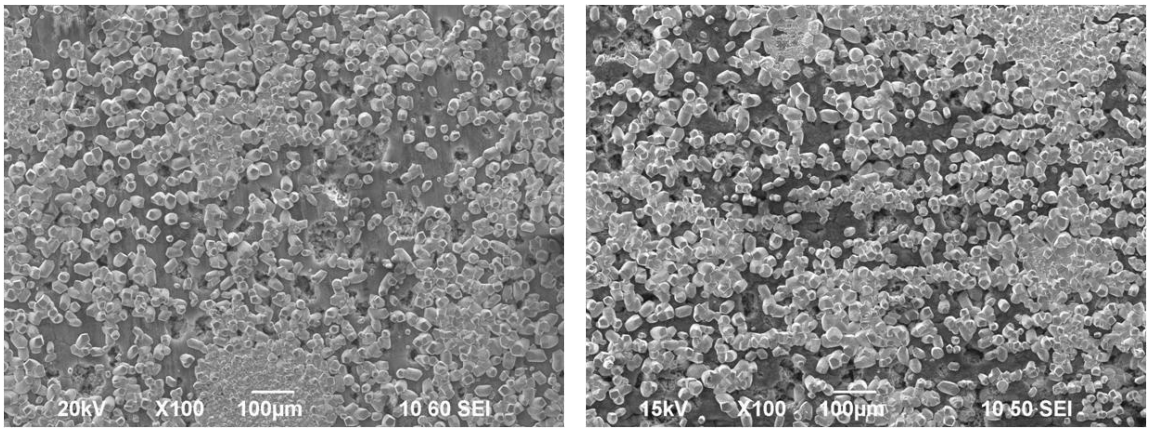

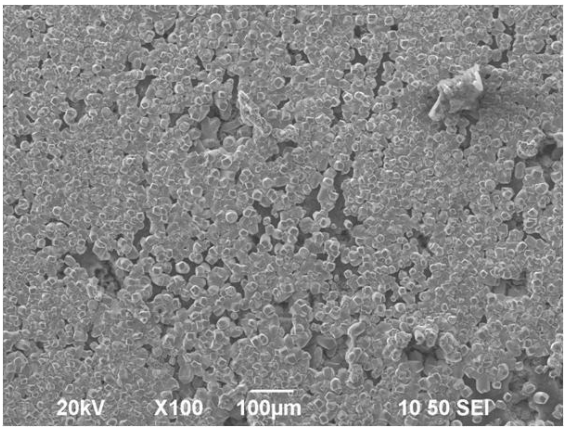

(c)

Figure 11: SEM images of the corroded surface of the sample exposed to a 25 wt.% NaCl solution at 90°C for 48 hours: (a) 4 MPa, (b) 8 MPa and (c) 12 MPa.

Figure 12 shows the XRD pattern of the corrosion product layers formed at 8 MPa, 90°C after 114 hours. Although the surface does not appear to be fully covered by $FeCO_3$ as shown in Figure 11 (b), it showed only $FeCO_3$ diffraction patterns.

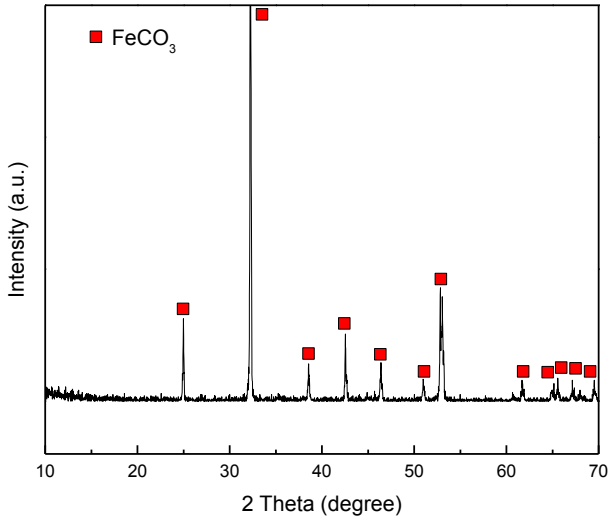

Figure 12. Result of XRD analysis for the sample exposed to 8 MPa, 90°C for 114 hours.

Figure 13 to Figure 15 represent the cross-sectional morphologies of the samples at different pressures. It can be seen from all three conditions that it has a "duplex" layer structure; outer Fe_3C layer with some $FeCO_3$ crystals and a thick/continuous inner $FeCO_3$ layer underneath the Fe_3C layer which was not seen in the tests at 65°C. In addition, thicker inner $FeCO_3$ layer formed at 8 and 12 MPa than at 4 MPa because of longer exposure time. Similar corrosion product morphologies have been observed recently under different experimental conditions.[18]

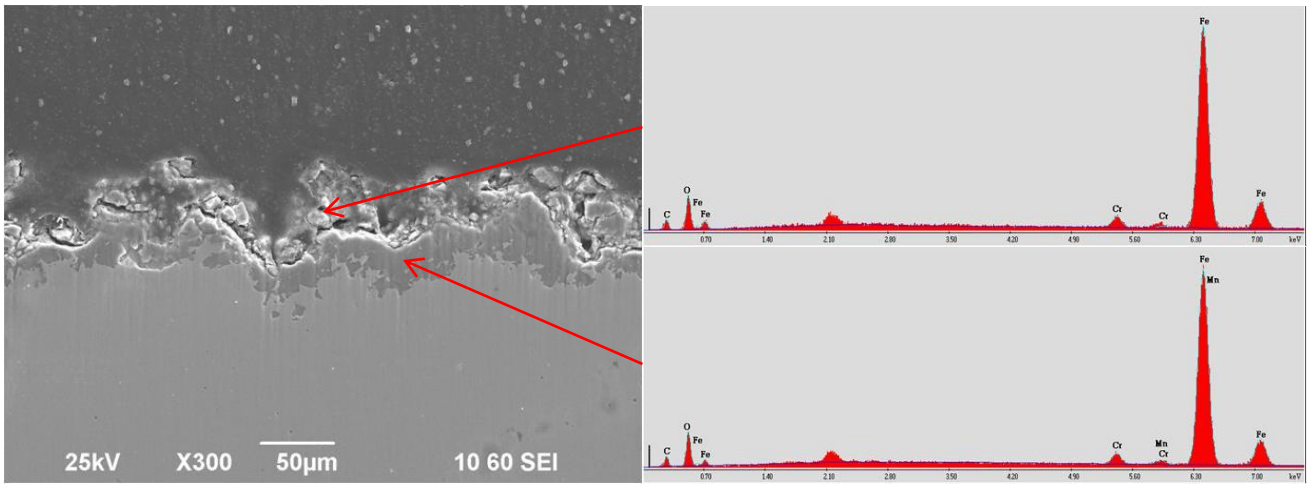

Figure 13: SEM image and EDS spectra of the cross-section of the sample exposed to 4 MPa and 90°C for 48 hours.

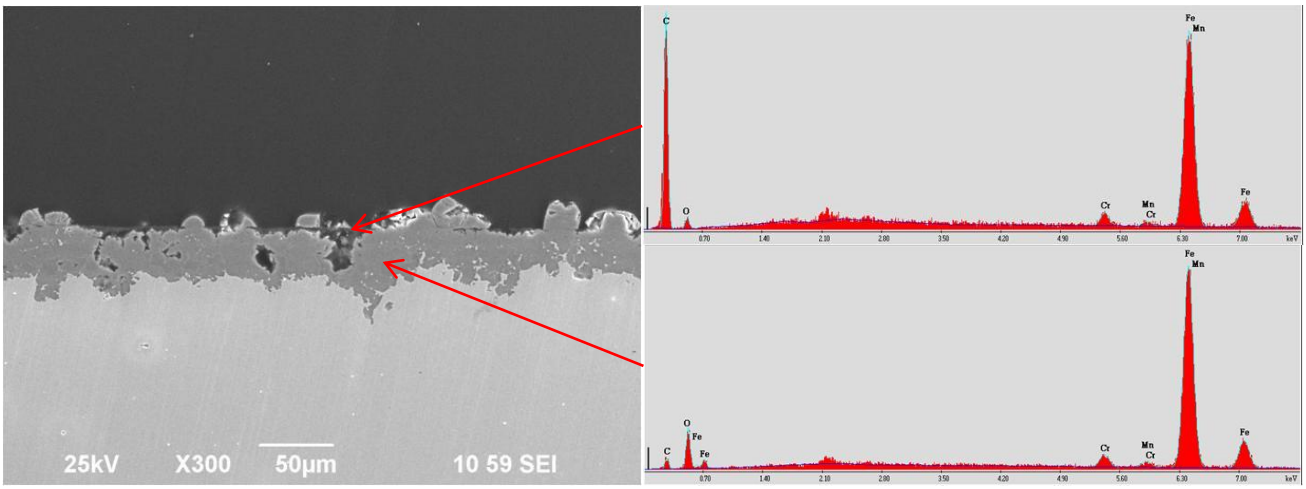

Figure 14: SEM image and EDS spectra of the cross-section of the sample exposed to 8 MPa and 90°C for 114 hours.

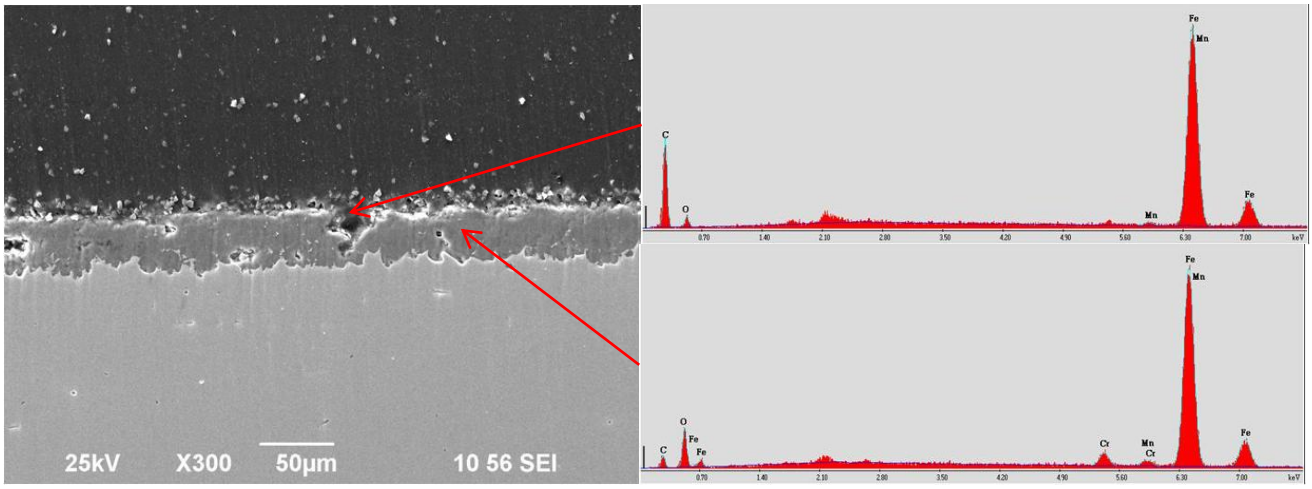

Figure 15: SEM image and EDS spectra of the cross-section of the sample exposed to 12 MPa and 90°C for 72 hours.

Furthermore, it is known that the nucleation and growth of the inner $FeCO_3$ typically starts at the steel surface, because of highest pH and $FeCO_3$ saturation values achieved there.[19] This is due to the Fe_3C layer restricting the transport of acidic species in and ferrous ions out, so the most favorable conditions for precipitation of a protective $FeCO_3$ layer are found inside the porous Fe_3C layer at the steel interface. The corrosion protection in the 90°C experiments was proved by the inner well attached and dense $FeCO_3$ layer which could not being seen from surface SEM observations, shown in Figure 11.

Figure 16 shows the surface morphologies of samples after removing the corrosion product layer with the Clarke solution. Pits are observed for all conditions. In order to examine their depth and calculate pit penetration rate, infinite focus microscope (IFM) analysis was performed for all samples.

Figure 17 shows results of IFM analysis for samples exposed to different CO_2 partial pressure at 90°C and Table 4 compares the corrosion rate obtained from weight loss measurements and IFM analysis. For all samples, the pit penetration rate calculated from the maximum pit depth showed higher values (2 ~ 3 times) than the time-averaged uniform corrosion rate which suggests initiation of localized corrosion.

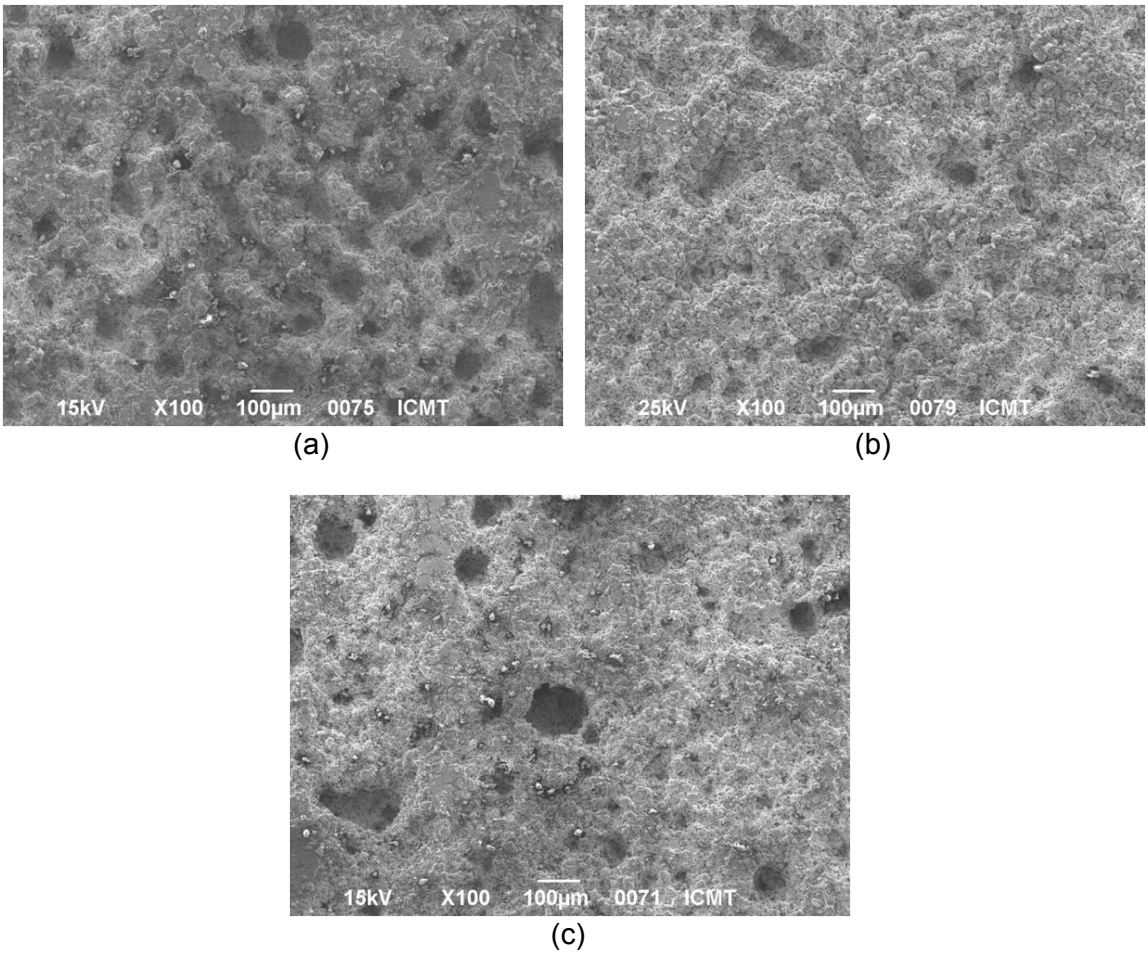

Figure 16: SEM images of the corroded surface of samples after cleaning: (a) 4 MPa, 90°C, (b) 8 MPa, 90°C and (c) 12 MPa, 90°C.

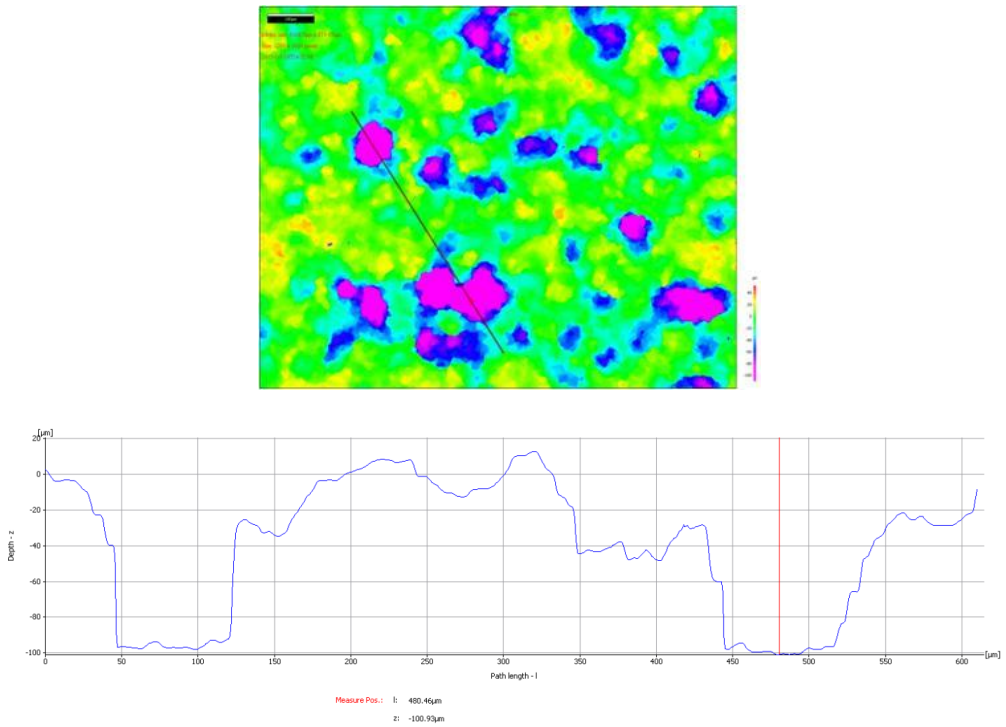

(a)

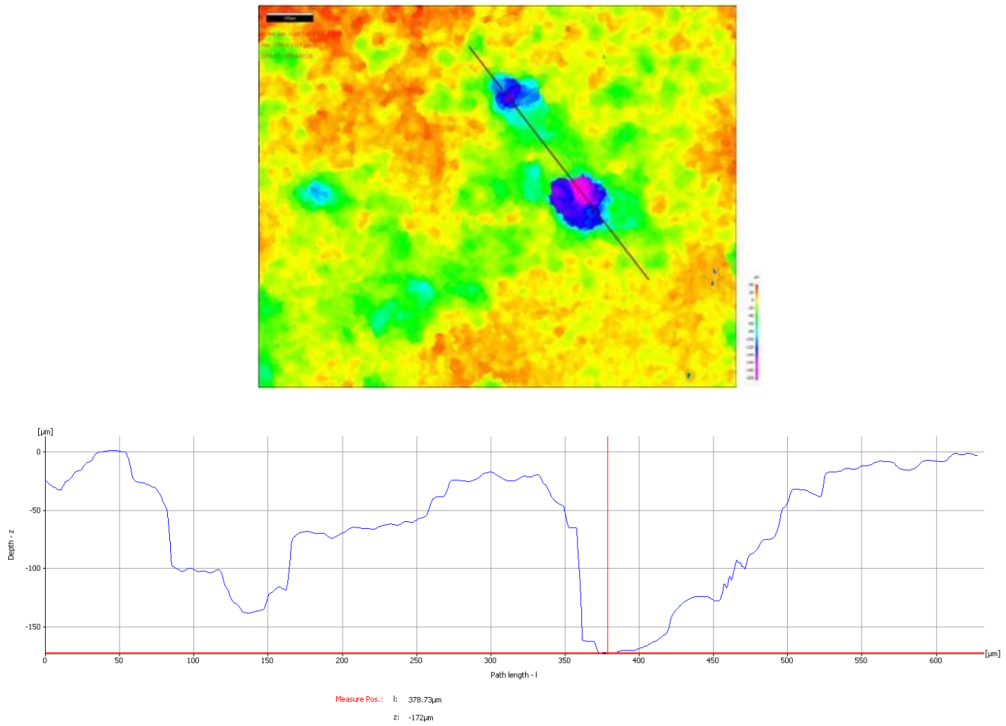

(b)

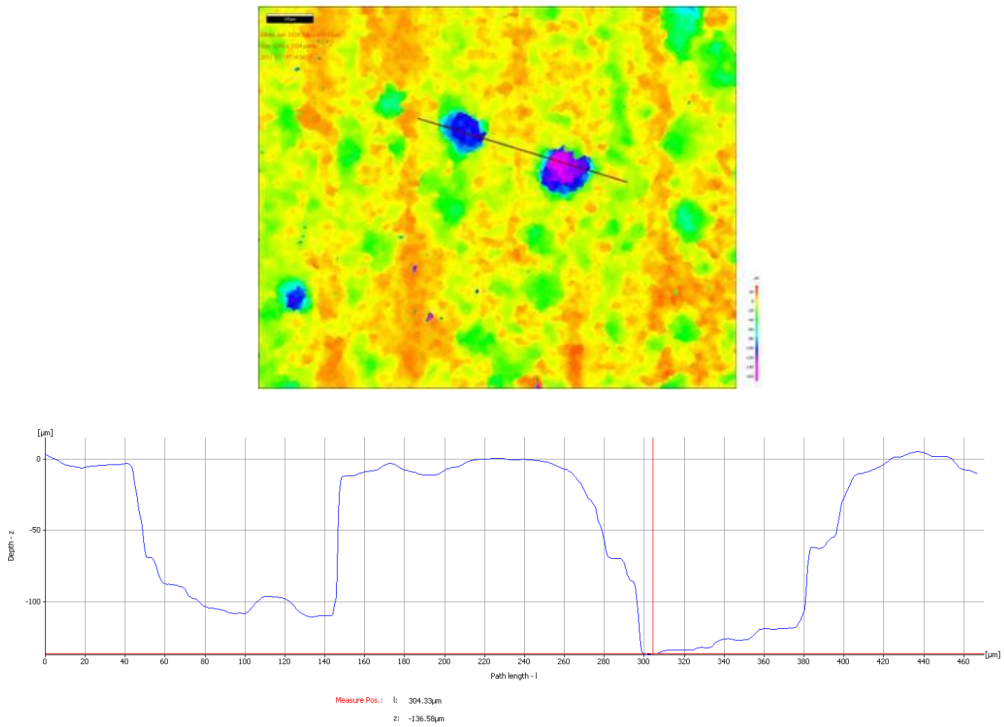

(c)

Figure 17: IFM surface analysis on cleaned surface of the sample: (a) 4 MPa, 90°C, (b) 8 MPa, 90°C, (c) 12 MPa, 90°C.

Table 4
Comparison of Corrosion Rates obtained from Weight Loss Measurements and IFM Analysis at 90°C

	Corrosion rate from weight loss (mm/y)	Maximum pit depth from IFM (µm)	Localized corrosion rate (mm/y)
4 MPa	5.5	100.9	18.4
8 MPa	5.6	172	13.2
12 MPa	7.3	136.5	16.6

* Exposure time: 48 hours (4 MPa), 114 hours (8 MPa), 72 hours (12 MPa)

CONCLUSIONS

- Uniform corrosion was observed at 65°C with a high corrosion rate (~ 10 mm/y) and little effect of CO2 partial pressure (at 4, 8 and 12 MPa). Under these conditions, the sample surface was locally covered by iron carbide (Fe_3C) which is porous and non-protective.
- The corrosion rates measured at 90°C started out higher but ended up being very low (≤ 0.1 mm/y) due to the formation of protective $FeCO_3$ layer regardless the CO_2 partial pressure. However, localized corrosion was seen with a maximum rate of 19 mm/y under this condition.

REFERENCES

1. L. P. Ribeiro, C. A. S. Paulo, E. A. Neto, “Compos Basin- Subsea Equipment: Evolution and Next Steps,” 2003 Offshore Technology Conference, Paper No. 15223, Offshore Technology Conference, Richardson, TX, 2003.

2. G. Estrella, “The Importance of Brazilian Deepwater Activities to the Oil Industry Technological Development,” 2003 Offshore Technology Conference, Paper No. 15049, Offshore Technology Conference, Richardson, TX, 2003.
3. J. R. F. Moreira, P. S. Rovina, P. Couto, B. Neumann, “Development and Installation of the Drill Pipe Riser, An Innovative Deepwater Production and Completion/Workover Riser System,” 1999 Offshore Technology Conference, Paper No. 10892, Offshore Technology Conference, Richardson, TX, 1999.
4. R. T. Hill, F. A. Ramirez, A. L. Perez, B. A. Monty, “Material Selection and Corrosion Control for Topside Process and Utility Piping and Equipment,” CORROSION/2012, paper no. 0001632 (Houston, TX: NACE International, 2012).
5. J. Carew, A. Al-Sayegh, A. Al-Hashem, “The Effect of Water-Cut on the Corrosion Behavior L80 Carbon Steel Under Downhole Conditions,” CORROSION/2000, paper no. 00061 (Houston, TX: NACE International, 2000).
6. J. Carew, A. Al-Hashem, “CO_2 Corrosion of L-80 Steel in Simulated Oil Well Conditions,” CORROSION/2002, paper no. 02299 (Houston, TX: NACE International, 2002).
7. H. J. Choi, D. K. Warnken, “Field Corrosion Assessment of L80 Carbon Steel Downhole Production Tubing in Khuff Gas Wells,” CORROSION/2006, paper no. 06653 (Houston, TX: NACE International, 2006).
8. Y. S. Choi, D. Young, S. Nesic, “Effect of Impurities on the Corrosion Behavior of CO_2 Transmission Pipeline Steel in Supercritical CO_2-Water Environment,” *Environ. Sci. Technol.* 44 (2010): p. 9233.
9. Y. S. Choi, S. Nesic, “Determining the Corrosive Potential of CO_2 Transport Pipeline in High pCO_2–Water Environments,” *International Journal of Greenhouse Gas Control* 5 (2011): p. 788.
10. Y. Zhang, X. Pang, S. Qu, X. Li, K. Gao, “The Relationship Between Fracture Toughness of CO_2 Corrosion Scale and Corrosion Rate of X65 Pipeline Steel Under Supercritical CO_2 Condition,” *International Journal of Greenhouse Gas Control* 5 (2011): p. 1643.
11. Y. Zhang, X. Pang, S. Qu, X. Li, K. Gao, “Discussion of the CO_2 Corrosion Mechanism Between Low Partial Pressure and Supercritical Condition,” *Corrosion Science* 59 (2012): p. 186.
12. M. F. Suhor, M. F. Mohamed, A. Muhammad Nor, M. Singer, S. Nesic, “Corrosion of Mild Steel in High CO_2 Environment: Effect of the $FeCO_3$ Layer,” CORROSION/2012, paper no. 0001434 (Houston, TX: NACE International, 2012).
13. Z. D. Cui, S. L. Wu, S. L. Zhu, X. J. Yang, “Study on Corrosion Properties of Pipelines in Simulated Produced Water Saturated with Supercritical CO_2,” *Applied Surface Science* 252 (2006): p. 2368.
14. F. Farelas, Y. S. Choi, S. Nesic, A. A. O. Magalhães, C. de Azevedo Andrade, “Corrosion Behavior of Deep Water Oil Production Tubing Material under Supercritical CO_2 Environment: Part 2. Effect of Crude Oil and Flow,” to be presented in CORROSION/2013 (Houston, TX: NACE International, 2013).
15. M. F. Mohamed, A. M. Nor, M. F. Suhor, M. Singer, Y. S. Choi and S. Nesic, “Water Chemistry for Corrosion Prediction in High Pressure CO_2 Environments,” CORROSION/2011, paper no. 11375 (Houston, TX: NACE International, 2011).
16. M. B. Kermani, A. Morshed, “Carbon Dioxide Corrosion in Oil and Gas Production- a Compendium,” *Corrosion* 59 (2003): p. 659.
17. J. Crolet, N. Thevenot, S. Nesic, “Role of Conductive Corrosion Products in the Protectiveness of Corrosion Layers,” *Corrosion* 54 (1998): p. 194.
18. T. Berntsen, M. Seiersten and T. Hemmingsen, Effect of $FeCO_3$ Supersaturation and Carbide Exposure on the CO_2 Corrosion rate of Carbon Steel, CORROSION/2011, paper no. 11072 (Houston, TX: NACE International, 2011).
19. F. Farelas, M. Galicia, B. Brown, S. Nesic, H. Castaneda, “Evolution of Dissolution Processes at the Interface of Mild steel Corroding in a CO_2 environment by EIS,” *Corrosion Science* 52 (2010): p. 509.